JOURNAL OF SYNCHROTRON RADIATION
ISSN 1600-5775

Enhancement of radiosensitivity of oral carcinoma cells by iodinated chlorin p_6 copper complex in combination with synchrotron X-ray radiation

Paromita Sarbadhikary[a,b] and Alok Dube[a,b]*

[a]Laser Biomedical Applications Section, Raja Rammana Centre for Advanced Technology, Indore, Madhya Pradesh 452013, India, and [b]Homi Bhabha National Institute, Training School Complex, Anushakti Nagar, Mumbai 400094, India. *Correspondence e-mail: okdube@rrcat.gov.in

Received 23 June 2017
Accepted 5 September 2017

Edited by R. W. Strange, University of Essex, UK

Keywords: chlorophyll derivative; DNA damage; radiosensitization; reactive oxygen species; synchrotron photon activation therapy.

Supporting information: this article has supporting information at journals.iucr.org/s

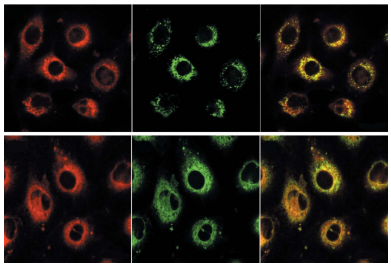

The combination of synchrotron X-ray radiation and metal-based radiosensitizer is a novel form of photon activation therapy which offers the advantage of treating malignant tumors with greater efficacy and higher precision than conventional radiation therapy. In this study the anticancer cytotoxic efficacy of a new chlorophyll derivative, iodinated chlorin p_6 copper complex (ICp_6-Cu), combined with synchrotron X-ray radiation (8–10 keV) in two human oral cancer cell lines is explored. Pre-treatment of cells with 20 µ*M* and 30 µ*M* ICp_6-Cu for 3 h was found to enhance the X-ray-induced cytotoxicity with sensitization enhancement ratios of 1.8 and 2.8, respectively. ICp_6-Cu localized in cytoplasm, mainly in lysosomes and endoplasmic reticulum, and did not cause any cytotoxicity alone. The radiosensitization effect of ICp_6-Cu accompanied a significant increase in the level of reactive oxygen species, damage to lysosomes, inhibition of repair of radiation-induced DNA double-strand breaks, increase in cell death and no significant effect on cell cycle progression. These results demonstrate that ICp_6-Cu is a potential agent for synchrotron photon activation therapy of cancer.

1. Introduction

Photon activation therapy (PAT) based on the photoactivation of a metal complex with synchrotron X-ray radiation is a promising approach for the treatment of chemo- and radio-resistant tumors (Adam *et al.*, 2008; Deman *et al.*, 2010; Gil *et al.*, 2011). Photoactivation of high-*Z* elements with an X-ray beam energy higher than the binding energy of the electrons leads to ionization of the atom or molecule and creation of an inner shell vacancy. Subsequently, the relaxation of the excited state results in the generation of photoelectrons and secondary electrons of very low energies (∼20–500 eV) *via* radiative and non-radiative processes known as the photoelectric effect and Auger effect, respectively. Both photoelectrons and Auger electrons can damage the nearby biomolecules directly and also cause radiolysis of water molecules resulting in the generation of cytotoxic free radicals (Kobayashi *et al.*, 2010). The sensitization effect of metal complexes results in higher dose deposition in tumor tissue and, since relatively low doses of radiation are required, damage to the normal tissue can be reduced significantly. Owing to this advantage, PAT is actively being investigated for the treatment of high-grade brain tumors with promising outcomes. For example, studies in glioma-bearing rats and mice have shown that administration of iodine or platinum compounds and their activation with X-rays results in larger tumor reduction and higher survival compared with radiation

alone (Biston *et al.*, 2004; Adam *et al.*, 2006, 2008; Rousseau *et al.*, 2009; Ricard *et al.*, 2013). Recently, Ceresa *et al.* (2014) reported that cisplatin plus irradiation with synchrotron radiation X-rays produces substantially higher cell killing compared with conventional X-ray irradiation in highly resistant glioblastoma multiforme cells. However, the use of cisplatin is associated with severe side effects which warrant development of less toxic and more effective agents to fully exploit the advantages of this therapeutic approach (Astolfi *et al.*, 2013). Some metal-nanoparticle-based radiation-dose enhancers such as gold (Hainfeld *et al.*, 2008; Su *et al.*, 2014), gadolinium (Taupin *et al.*, 2015), iron (Choi *et al.*, 2012) and tantalum oxide (Engels *et al.*, 2017) have also been investigated for PAT.

The propensity of porphyrin and chlorin derivatives to accumulate preferentially in tumor has been successfully exploited for the photodynamic therapy (PDT) of cancer (Abrahamse & Hamblin, 2016). However, due to the low penetration depth of light in tissue, PDT is not effective for deep-seated tumors. Recently, a novel therapeutic approach that utilizes X-ray radiation to activate photosensitizer (PS) directly or indirectly through absorption of X-ray energy by high-Z elements has gained considerable attention (Ishibashi *et al.*, 2013; Chen *et al.*, 2015; Kaščáková *et al.*, 2015; Wang *et al.*, 2016). One such approach requires activation of PS indirectly *via* X-ray-induced luminescence of metal nanoparticles or lanthanide atoms such as europium or terbium, placed in close vicinity of the PS (Liu *et al.*, 2008). The efficacy of this approach depends on several factors such as the effective energy transfer between PS and the scintillating material, the cellular uptake of the conjugate, and most importantly the singlet oxygen yield which in deeper tumor regions will be limited by hypoxic conditions (Chapman *et al.*, 1991; Moan & Sommer, 1985; Morgan *et al.*, 2009). Alternatively, a therapeutic approach based on the direct X-ray photoactivation of metal conjugated PS can be more suitable for the treatment of deep-seated tumors, because it acts *via* free-radical generation which is less likely to be affected by hypoxia. So far, only a few metal conjugated PSs such as gold complex of chlorin e6 (Tsuchida *et al.*, 2003) and iodinated pyropheophorbide derivative (Ishibashi *et al.*, 2013) have been investigated for the X-ray photoactivation treatment of cancer.

Recently, we have reported a novel metal complex of chlorin p_6 referred to as iodinated chlorin p_6 copper complex (ICp_6-Cu) for potential use in PDT of cancer. ICp_6-Cu demonstrated pronounced photodynamic activity *via* free-radical generation and induced potent phototoxic effect against cancer cells under both normoxic and hypoxic conditions (Sarbadhikary *et al.*, 2016). The presence of copper and iodine in ICp_6-Cu makes it suitable for X-ray photoactivation using an X-ray energy of $\geq$8.9 keV or $\geq$33.2 keV, respectively. While a lower X-ray energy ($\sim$9 keV) due to low tissue penetration (half value layer $\sim$1.0 mm) can be used for superficial tumors, higher-energy X-rays ($\sim$33 keV) due to better tissue penetration (half value layer $\sim$2.0 cm) can be exploited for deeper tumor treatment. In the present study we explored the efficacy of ICp_6-Cu for X-ray photoactivation-induced cytotoxicity in two human oral cancer cell lines. The effects of synchrotron X-ray radiation (8–10 keV) without and with ICp_6-Cu treatment on cell viability and colony forming ability of cancer cells were examined. Studies on cellular reactive oxygen species (ROS) levels, intracellular localization of ICp_6-Cu, DNA damage and cell cycle progression were performed to understand the mode of ICp_6-Cu-induced radiosensitization.

2. Materials and methods

2.1. Materials

ICp_6-Cu was prepared from Cp_6 following the procedure described in our Indian patent application (No. 4912/MUM/2015). Stock solution of concentrated ICp_6-Cu (molecular weight 792) was made in ethanol:PEG (400):water (20:30:50) and used in experiments.

The fluorescence organelle probes mito tracker green, lyso tracker blue, ER tracker green and Golgi tracker green were obtained from Thermo Fischer Scientific, USA. 2′,7′-Dichlorodihydrofluorescin diacetate (DCFH-DA), Hoechst 33342 (HO), propidium iodide (PI), and Dulbecco's modified eagle's medium (DMEM) were purchased from Sigma, USA. Phosphate-buffered saline (PBS), tetrazolium salt 3-(4,5-dimethylthiazol-2-yl)-2,5-diphenyltetrazolium bromide (MTT), trypsin/EDTA and fetal bovine serum (FBS) were obtained from Himedia, India. All other solvents and reagents used were of analytical grade.

2.2. Cell culture

Two oral carcinoma cell lines, NT8e and 4451, obtained from ACTREC, Mumbai, India, and INMAS, Delhi, India, respectively, were maintained in DMEM containing antibiotics (streptomycin, nystatin and penicillin) and 10% FBS. Cells were grown at 37°C under 5% CO_2 + 95% air atmosphere in a humidified incubator (ESCO). The cells after 80% confluent growth were harvested by trypsinization and plated either in flat-bottomed 96-well plates, 24-well plates or glass-bottom pertidishes. The cells were allowed to grow for 18 h and then used for the experiments.

2.3. Cellular uptake of ICp_6-Cu

The monolayer of cells ($\sim 2 \times 10^5$ cells) grown in a 24-well plate were incubated in DMEM medium containing 10, 20 and 30 µM ICp_6-Cu for 3 h at 37°C, in the dark. The cells were washed twice with PBS and solubilized in 200 µl detergent solution (0.1 M NaOH + 0.1% SDS) by scrapping and repeated pipetting. After centrifugation (10000 r.p.m., 10 min), absorption of the cell extract at 640 nm was measured on a plate reader (Power Wave 340, Bio-tek instruments Inc., USA). The protein content of each sample was determined by bicinchoninic acid protein assay (Sapan *et al.*, 1999) and a standard curve of ICp_6-Cu prepared in NaOH/SDS solution was used to calculate the amount of ICp_6-Cu in cells (nM µg^{-1} of protein).

2.4. Intracellular localization of ICp_6-Cu

The distribution of ICp_6-Cu in various cell organelles was studied by fluorescence imaging using an LSM 880 confocal microscope (Carl Zeiss, Germany). The cells grown on glass-bottom petriplates were incubated with 10 µ*M* ICp_6-Cu in DMEM medium for 3 h at 37°C, in the dark. The cells were then washed twice with PBS and stained with either ER tracker green, mito tracker green, lyso tracker blue, Golgi tracker green or HO. The localization of ICp_6-Cu in cells was imaged by excitation with a 405 nm diode laser and collection of the emitted fluorescence using a 570 nm long-pass filter on a high-sensitivity GaAsP detector. HO and lyso tracker blue were excited with the 405 nm laser and fluorescence emission from 420 nm to 480 nm was imaged on a photomultiplier tube (PMT) detector. Mito, Golgi and ER tracker probes were excited at 488 nm with argon ion laser and the emitted fluorescence emission from 490 nm to 560 nm was recorded on the PMT detector.

2.5. ICp_6-Cu treatment and X-ray irradiation

NT8e and 4451 cells grown in 96-well plates were incubated in growth medium containing ICp_6-Cu for 3 h, in the dark. The cell monolayers were washed twice with DMEM (without serum) and, subsequent to the addition of fresh DMEM, were exposed to X-ray radiation (8–10 keV) using beamline BL7 of the Indus-II synchrotron source at Raja Ramanna Centre for Advanced Technology, Indore, India. A photograph of the experimental setup is shown in Fig. 1(*a*). The X-ray energy was tuned in the range 8–10 keV (Fig. 1*b*) by inserting a 396 µm-thick aluminium filter into the beam path. For irradiation, the 96-well plate was mounted vertically on a motorized stage in front of the source. The beam size was 3.5 mm × 70 mm to allow simultaneous irradiation of six wells horizontally. The variation in photon flux of the beam in the horizontal direction was <7.0%. Further, the stage was translated in the vertical direction to ensure homogeneous exposure. Absorbed X-ray doses were determined using the xylenol orange Fricke dosimetry method (Gohary *et al.*, 2015). The dose rate computed from a plot of the change in absorbance of xylenol orange Fricke solution *versus* number of scans was ∼33.5 ± 0.6 cGy scan^{-1} (see Fig. S1 of the supporting information). An X-ray dose of 1–17 Gy was delivered by varying the number of scans. To take into account the ring current variation, prior to each exposure (samples in a 96-well plate) the scan translation speed of the stage was adjusted in the range from 7 mm s^{-1} to 9 mm s^{-1} with respect to the value of the ring current variation. Further, to minimize the day-to-day variation, the experiments were performed when the ring current was between 90 and 120 mA. For this, the time to initiate the sample preparation was adjusted accordingly. In addition, prior to each experiment, a 96-well plate containing xylenol orange Fricke solution was also exposed to X-rays to ensure that the dose delivered was almost the same in different experiments.

2.6. Cell cytotoxicity assay

After X-ray irradiation, the cells were washed with DMEM (without serum) and allowed to grow for 96 h at 37°C under 5% CO_2 + 95% air atmosphere. Subsequently, X-ray-induced cytotoxicity without and with ICp_6-Cu pre-treatment was determined by MTT assay (Price & McMillan, 1990). In live cells, MTT is converted into dark blue formazan through enzymatic action of mitochondrial succinate dehydrogenase and the optical density of the color produced is used to determine the relative number of viable cells (Mosmann, 1983). To perform this assay, the growth medium from the cells was replaced with DMEM (without serum) containing 0.5 mg ml^{-1} MTT. After incubation at 37°C for 3 h in the dark, the medium was removed and 100 µl DMSO was added to dissolve the formazan crystals formed within the cells. The absorbance of the samples at 570 nm with reference wavelength at 690 nm was read using a microplate reader. The percent cytotoxicity was calculated with respect to the absorbance value of the control samples.

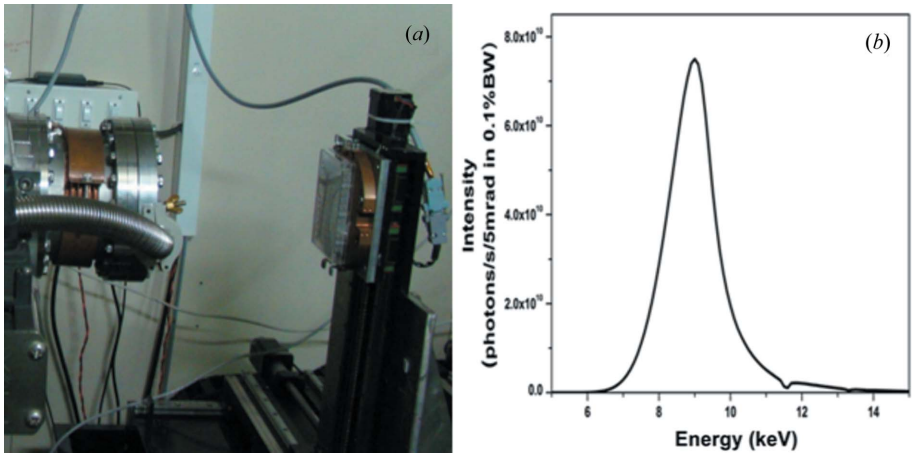

Figure 1
(*a*) Experimental set-up at the X-ray lithography beamline (BL7) used for X-ray irradiation of cells in a 96-well plate. The plate was mounted vertically onto a motorized stage in front of the beam (beam size of 3.5 mm × 70 mm). (*b*) Calculated spectrum of synchrotron X-rays in the energy range 8–10 keV.

2.7. Clonogenic survival assay

The sensitizer enhancement ratio (SER) at 7 Gy was determined by clonogenic survival assay. Cells were seeded in 24-well plates (∼100 cells per well) and allowed to attach overnight. Then cells were treated with ICp_6-Cu (10, 20, 30 µ*M*) for 3 h and then irradiated with X-rays at a fixed dose of 7 Gy which was predetermined from cytotoxicity experiments. After irradiation, the cells were washed with DMEM media (without serum) and allowed to grow for 10–14 days to form colonies.

The colonies were fixed in 4% paraformaldehyde, stained with crystal violet and then counted. The surviving fraction (SF) was calculated as

$$\mathrm{SF} = \frac{\text{mean number of colonies formed after treatment}}{\text{number of cells seeded} \times \mathrm{PE}}, \quad (1)$$

where PE (the plating efficiency) was determined as

$$\mathrm{PE} = \frac{\text{mean number of colonies formed in untreated control}}{\text{number of cells seeded}} \times 100, \quad (2)$$

$$\mathrm{SER\,(7\,Gy)} = \frac{\text{SF at 7 Gy of radiation alone}}{\text{SF at 7 Gy of radiation} + \mathrm{IC}p_6\text{-Cu}}. \quad (3)$$

2.8. Detection of ROS generation

The relative level of intracellular ROS in cells was measured by fluorescence spectroscopy using the fluorescent probe DCFH-DA. The non-fluorescent DCFH-DA freely diffuses in cells and converted into a non-fluorescent product 2′,7′-dichlorodihydrofluorescein (DCFH) by the enzymatic action of cellular esterases. In cells, DCFH reacts with ROS to yield a highly fluorescent product dichlorofluorescein (DCF). The fluorescence intensity of DCF in cells is directly proportional to the level of ROS (Rappole *et al.*, 2012). To perform this assay, the cells after X-ray irradiation were incubated at 37°C for 30 min in DMEM (without serum) containing 10 µ*M* DCFH-DA. Cells were released by trypsinization, re-suspended in PBS and the fluorescence of DCF in cell suspension was measured on a spectrofluorometer (model Fluorolog-2; Spex, USA) using a 488 nm excitation wavelength and 525 nm emission wavelength with a band pass of ∼1.7 nm and ∼3.7 nm, respectively. The fluorescence intensity of DCF in the control and different treatment groups after normalization with the cell number was used to express the relative ROS levels.

2.9. γ-H2AX immunofluorescence

The effect of X-ray irradiation either alone or combined with ICp_6-Cu treatment (30 µ*M*, 3 h) on DNA damage and repair in oral cancer cells was determined by γ-H2AX immunofluorescence, which is a reliable and sensitive biomarker for the detection of DNA double-strand breaks (DSBs) (Mah *et al.*, 2010). For this, cells were grown on X-ray transparent Kapton film and, subsequent to X-ray exposure (∼7.0 Gy), were fixed in 4% paraformaldehyde for 15 min at room temperature. The cells were washed three times with PBS, permeablized by treatment with 0.5% Triton X-100 for 5 min. After washing three times with PBS the cells were treated with 5% BSA solution for 1 h to block non-specific binding sites. The cells were then incubated with mouse anti-human γ-H2AX antibody (Millipore, dilution 1:200) for 1.5 h, washed twice with 0.05% Tween-20 in PBS and incubated with Alexa Fluor 488 labeled rabbit anti-mouse antibody (Invitrogen, dilution 1:400) for 1 h. After a final wash with PBS for 10 min, cells were counterstained with DAPI (1 µg ml^{-1}) for 5 min and the fluorescence in the cells was examined on a Zeiss LSM 880 confocal microscope. Alexa Fluor was excited at 488 nm and its fluorescence was recorded in channel 1 with a bandpass of 490–560 nm. DAPI was excited at 405 nm and its fluorescence in the wavelength range 420–480 nm was recorded in channel 2. Images were captured using 40× (numerical aperture 1.3) objective and analyzed by *Image J* software to count the number of γ-H2AX foci in each cell. For each treatment and control, at least 100 cells were analyzed to obtain the value of the number of foci per cell.

2.10. Cell cycle analysis

The effect of X-ray irradiation without and with ICp_6-Cu pre-treatment on cell cycle and cell death was assessed by flow cytometry. After X-ray irradiation, the cells were allowed to grow for 24 h and then the non-adherent cells in media were collected by centrifugation and the adherent cells were released by trypsinization. The adherent and non-adherent cells were mixed, washed with PBS, re-suspended in ice-cold 70% ethanol and stored at 4°C until analysis. For flow cytometry measurements, the cells were centrifuged, washed in PBS and re-suspended in 1.0 ml PBS containing 50 µg ml^{-1} PI. The cells were kept at 4°C in the dark for ∼18 h, and the DNA content in the cells was measured on a Cyflow cytometer (Partec, Germany). The percentage of cells in G1, S and G2/M phases of the cell cycle were analyzed from DNA histograms. The sub-G1 hypodiploid DNA content peak in the histogram was used to determine the apoptotic population (Darzynkiewicz *et al.*, 2010).

2.11. Statistical analysis

All the experiments were performed at least three times using three replicates in each experiment. The data obtained from three independent experiments were plotted as mean ± standard deviation and a Student's t-test was applied for comparisons between different treatments. $p < 0.05$ was considered to be statistically significant.

3. Results

3.1. Intracellular uptake and localization of ICp_6-Cu

As shown in Fig. 2, both NT8e and 4451 cells accumulated a significant amount of ICp_6-Cu after 3 h incubation. The cellular level of ICp_6-Cu was found to increase with concentration and, as compared with NT8e cells, 4451 cells showed significantly higher accumulation of ICp_6-Cu at 20 µ*M* and 30 µ*M*. Next, we examined the intracellular distribution of ICp_6-Cu in NT8e cells. In Fig. 3 the confocal microscopic image of NT8e cells showing the fluorescence of ICp_6-Cu together with cell organelle probes ER and lyso tracker are presented. The red fluorescence of ICp_6-Cu was observed mainly in cytoplasm [Figs. 3(*a*) and 3(*d*)]. The green fluorescence of lyso tracker as well as ER tracker is well demarcated [Figs. 3(*b*) and 3(*e*)] which overlapped considerably with the

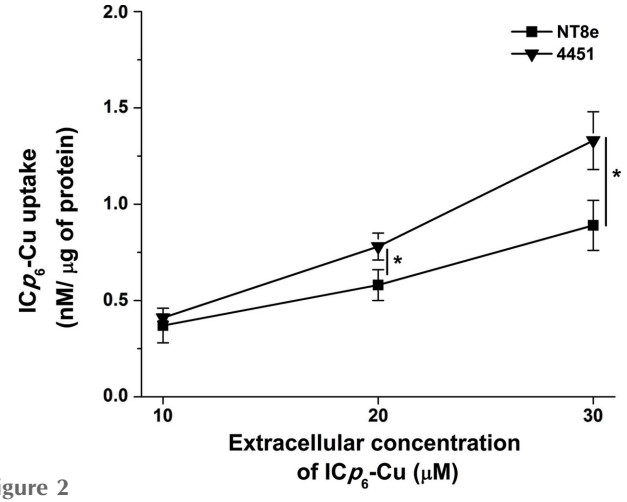

Figure 2
Intracellular uptake of ICp_6-Cu as a function of concentration in NT8e and 4451 cells. Data are mean ± standard deviation of three independent experiments.

red fluorescence of ICp_6-Cu as indicated by yellow regions in the overlay images [Figs. 3(*c*) and 3(*f*)]. With mito and Golgi specific fluorescence probes, the fluorescence of ICp_6-Cu did not show significant overlap (data not shown). These observations showed that ICp_6-Cu localized mainly in lysosomes and ER.

3.2. ICp_6-Cu pre-treatment enhances X-ray-induced cytotoxicity

The effect of ICp_6-Cu pre-treatment on X-ray-induced cytotoxicity in NT8e and 4451 cells is shown in Fig. 4. In both of the cell lines, X-ray irradiation led to a dose-dependent decrease in cell viability wherein ∼50% and 90% cytotoxicity was observed at ∼10 Gy and ∼17 Gy, respectively. In 4451 cells, pre-treatment with 10 μ*M* ICp_6-Cu led to a significant increase in X-ray-induced cytotoxicity at X-ray doses ≥ 7.0 Gy (Fig. 4*b*), whereas, in NT8e cells, pre-treatment with 10 μ*M* ICp_6-Cu did not lead to any significant increase in X-ray-induced cytotoxicity at any dose (Fig. 4*a*). At 20 μ*M*, ICp_6-Cu led to a significant increase in X-ray-induced cytotoxicity ($p < 0.05$) in both of the cell lines, and the magnitude of the effect was observed to increase further with increase in concentration of ICp_6-Cu. At 7 Gy X-ray dose, the loss of cell viability in 4451 cell was ∼38% which increased to ∼48%, ∼64% and ∼78% in cells pre-treated with 10 μ*M*, 20 μ*M* and 30 μ*M* ICp_6-Cu, respectively. In NT8e cells, a similar concentration-dependent increase in X-ray-induced cytotoxicity was seen but the magnitude of the effect was significantly lower ($p < 0.05$) than that for 4451 cells (Fig. 4*c*). At 7 Gy X-ray dose, the loss of cell viability in NT8e cells was ∼42% which increased to ∼47%, ∼56% and ∼67% in cells pre-treated with 10, 20 and 30 μ*M* ICp_6-Cu, respectively.

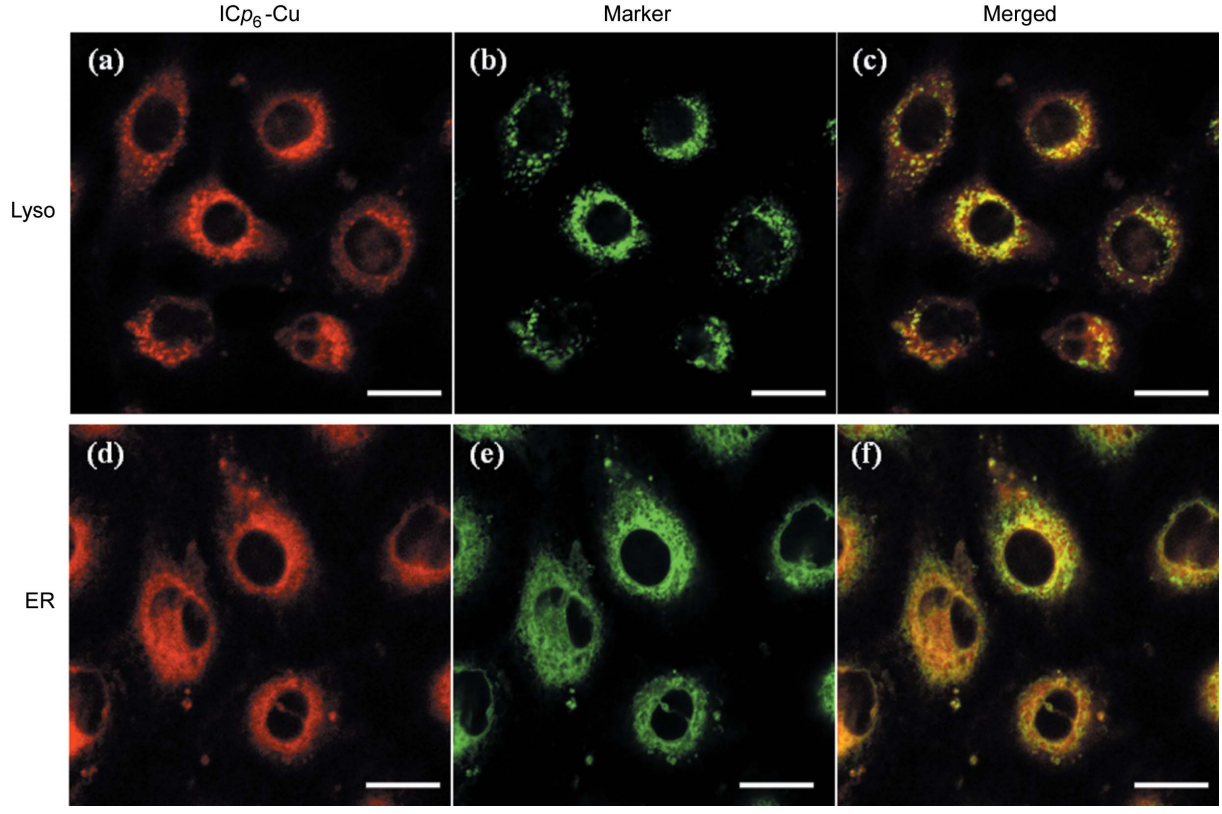

Figure 3
Localization of ICp_6-Cu in NT8e cells. Confocal fluorescence micrographs of NT8e cells showing red fluorescence of ICp_6-Cu (*a*, *d*), and green fluorescence of lysotracker (*b*), ER tracker (*e*) and the merged image of ICp_6-Cu and the organelle probes (*c*, *f*). Experiments were repeated three times with similar results and representative images are shown. Magnification 40×; scale bar 20 μm.

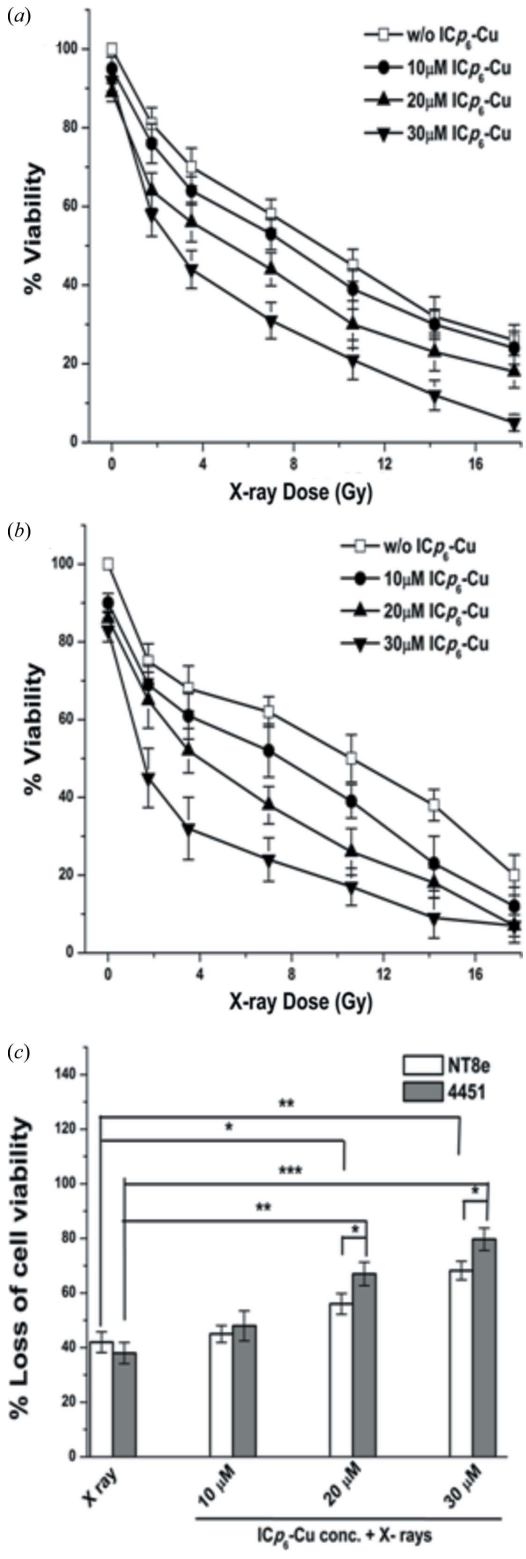

Figure 4
Cytotoxic effects of X-rays without and with ICp_6-Cu pre-treatment in oral cancer cells determined by MTT assay. Changes in percent cell viability in NT8e (*a*) and 4451 (*b*) cells as a function of X-ray dose; the cells were pre-treated with 10, 20 and 30 μ*M* ICp_6-Cu for 3 h. Percent cell viability was calculated with respect to a control sample (without ICp_6-Cu treatment). (*c*) Percent loss of cell viability in NT8e and 4451 for X-rays alone and X-rays plus ICp_6-Cu at 7 Gy X-ray dose. *($p < 0.05$), **($p < 0.01$), ***($p < 0.005$) indicate significant difference. Each data point is mean ± standard deviation of three independent experiments.

3.3. X-ray dose enhancement effect by ICp_6-Cu

The effect of X-rays alone (7 Gy) and ICp_6-Cu plus X-ray treatment on the percent cell survival of NT8e and 4451 cells is shown in Fig. 5(*a*). Compared with X-rays alone, ICp_6-Cu plus X-ray treated cells shows a greater decrease in the surviving fraction and the magnitude of the effect increased with an increase in the concentration of ICp_6-Cu (Fig. 5*a*).

The SER obtained from the cell survival data for NT8e cells was ∼1.0, 1.7 and 2.68 at 10 μ*M*, 20 μ*M* and 30 μ*M* ICp_6-Cu, respectively (Fig. 5*b*). Consistent with the MTT assay, the radiosensitization effect of ICp_6-Cu was more pronounced in 4451 cells than that for NT8e cells. SER values for 4451 cells

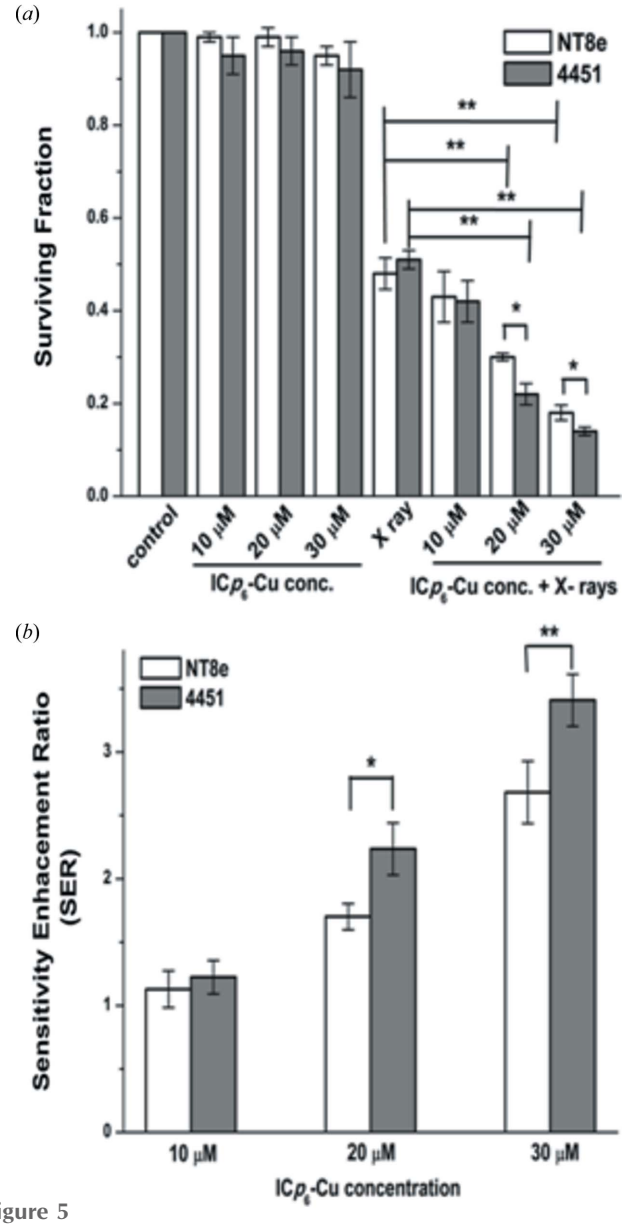

Figure 5
Radiosensitization effect of ICp_6-Cu in oral cancer cells determined by clonogenic assay. (*a*) Surviving fraction and (*b*) sensitivity enhancement ratio (SER) in NT8e and 4451. The cells were treated with ICp_6-Cu (10, 20 and 30 μ*M*) for 3 h and then irradiated with X-rays at a fixed dose of 7.0 Gy. *($p < 0.05$) and **($p < 0.01$) indicate significant difference. Data are mean ± standard deviation of three independent experiments.

were ~1.0, 2.23 and 3.4 at 10 μ*M*, 20 μ*M* and 30 μ*M* ICp_6-Cu, respectively. At 20 and 30 μ*M*, the values of SER for 4451 cells are significantly higher than those for NT8e cells ($p < 0.05$).

3.4. Enhancement in X-ray-induced ROS formation by ICp_6-Cu

The effect of X-ray irradiation on the relative level of ROS in 4551 and NT8e cells without and with ICp_6-Cu pre-treatment is shown in Fig. 6. Results show that, compared with control, X-ray irradiation alone led to only a marginal increase in the intracellular level of ROS ($p < 0.05$) in both of the cell lines. The level of ROS in the combination group increased significantly relative to the X-rays alone, with a more pronounced increase in cells pre-treated with 20 μ*M* and 30 μ*M* ICp_6-Cu. These results correlated with the enhancement in X-ray-induced cytotoxicity supporting the radiosensitization efficacy of ICp_6-Cu.

3.5. DNA damage induction and repair

The formation of DSBs and its repair play a significant role in X-ray-induced cytotoxicity. γ-H2AX, a DNA damage-sensing protein, is a most reliable marker for radiation-induced DNA damage (Mah *et al.*, 2010). Microphotographs of 4451 and NT8e cells showing the presence of γ-H2AX foci at 30 min, 2 h and 24 h after X-ray (7 Gy) irradiation are presented in Fig. 7. As expected, cells in control and ICp_6-Cu treatment did not show γ-H2AX foci [Figs. 7(*a*)-(i) and 7(*a*)-(ii)]. In contrast, cells irradiated with X-rays either without or with ICp_6-Cu pre-treatment displayed a large number of γ-H2AX foci within 30 min after irradiation. At this time, the number of γ-H2AX foci in X-rays alone and ICp_6-Cu plus X-ray irradiated cells was almost equal (Fig. 7*b*) indicating that pre-treatment with ICp_6-Cu did not affect X-ray-induced DNA damage. At 2 h and 24 h post-irradiation, the number of γ-H2AX foci in X-ray-irradiated cells declined to ~40% and ~15%, respectively, indicating repair of DSBs [Figs. 7(*c*)-(i) and 7(*c*)-(ii)], whereas in cells treated with ICp_6-Cu plus X-ray irradiation the number of γ-H2AX foci decreased to a lesser extent by ~60% at 2 h and thereafter no significant decrease was observed [Figs. 7(*c*)-(i) and 7(*c*)-(ii)]. These results showed that DNA repair is impaired due to combined treatment. Moreover, the number of γ-H2AX foci at 24 h after combined treatment was higher in 4451 cells than for NT8e cells (Fig. 7*c*) which was consistent with the higher radiosensitivity of 4451 cells.

3.6. Radiation-induced cell organelle damage

Since ICp_6-Cu localized in lysosomes and ER, the possibility of damage to these vital organelles was studied by confocal fluorescence microscopy. In Fig. 8, microphotographs of NT8e cells in control, ICp_6-Cu alone, X-ray irradiated and ICp_6-Cu plus X-ray irradiated cells are shown. In control, ICp_6-Cu alone and X-ray irradiation, lysosomes are intact as indicated by well demarcated punctuate fluorescence [Figs. 8(*a*), 8(*b*) and 8(*c*)]; whereas in cells that received combined treatment the fluorescence of lysotracker was diffuse and less intense indicating disintegration of lysosomes [Fig. 8(*d*)]. X-ray irradiation alone or ICp_6-Cu plus X-rays led to no significant

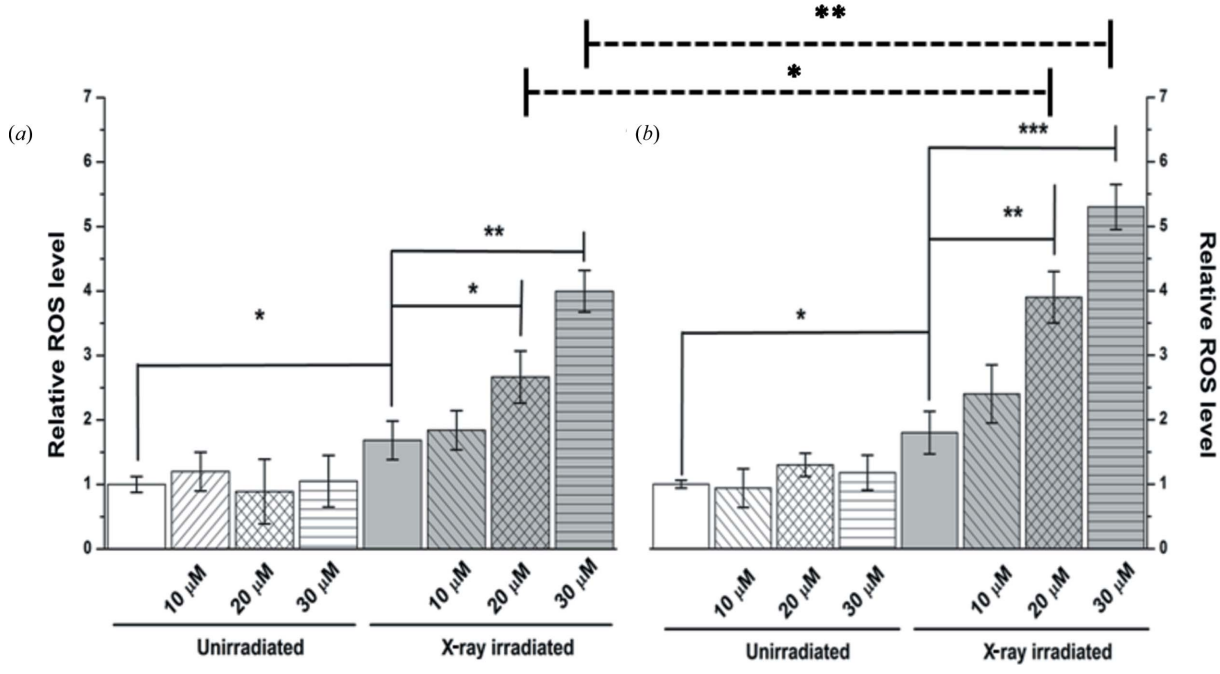

Figure 6
Effects of ICp_6-Cu and X-ray irradiation on ROS formation. Relative levels of ROS after X-ray irradiation (7 Gy), in NT8e (*a*) and 4451 (*b*) without or with ICp_6-Cu pre-treatment. Data are mean ± standard deviation of three independent experiments. *($p < 0.05$), **($p < 0.01$), ***($p < 0.005$) indicate statistical significance.

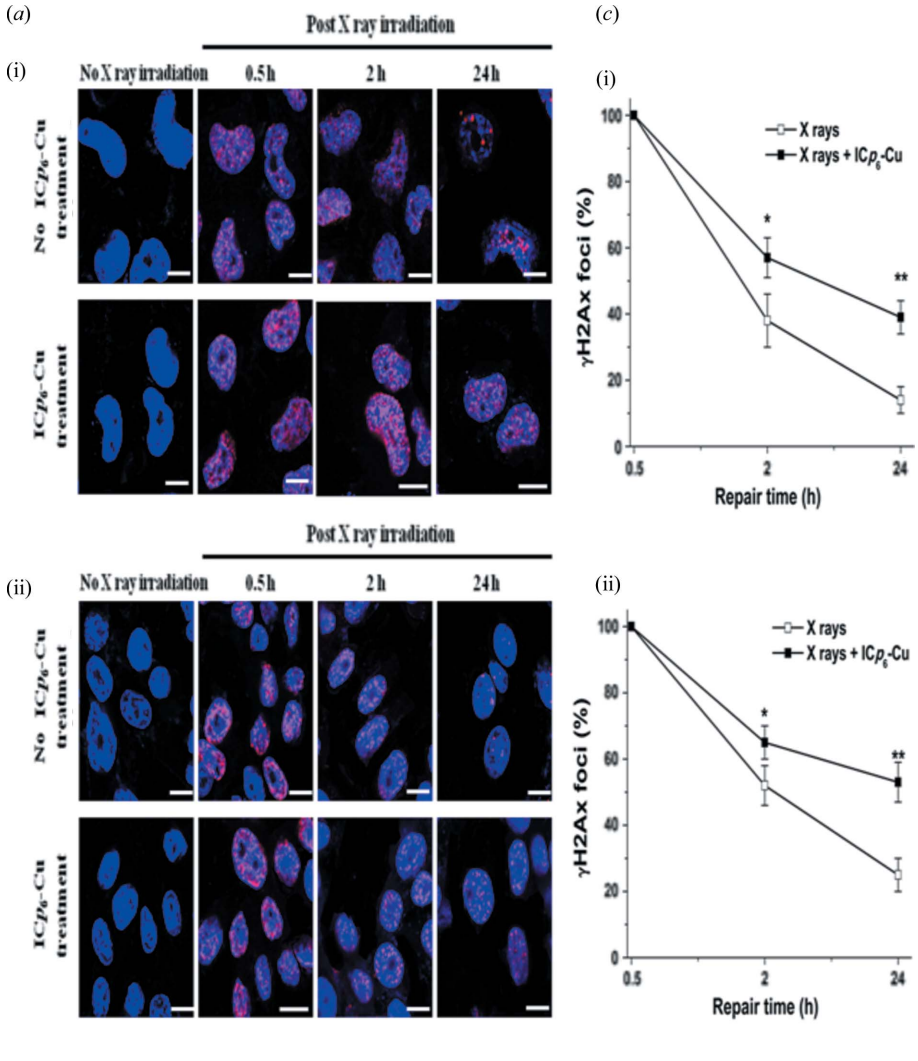

(b)

Cell line	X-rays	X-ray + ICp_6-Cu
NT8e	120 ± 26	133 ± 33
4451	74 ± 12	77 ± 14

Figure 7
Effect of ICp_6-Cu and X-ray irradiation on DNA damage determined by γ-H2AX immunostaining. (*a*) Representative immunofluorescence images of NT8e (i) and 4451 (ii) cells treated without (upper panel) or with (lower panel) 30 µ*M* ICp_6-Cu at various time points post-irradiation (7 Gy). Images show cell nuclei in blue and γ-H2AX foci in red. (*b*) Number of γ-H2AX foci at 30 min post-irradiation (7 Gy) in NT8e and 4451 cells without or with ICp_6-Cu treatment (30 µ*M*). (*c*) Changes in percentage of γ-H2AX foci in NT8e (i) and 4451 (ii) cells treated with or without 30 µ*M* ICp_6-Cu at different time periods post-irradiation (7 Gy), indicating repair kinetics of DSBs. Data represent mean ± standard deviation obtained from three independent experiments. *($p < 0.05$), **($p < 0.01$) indicate statistical significance between X-rays alone and ICp_6-Cu plus X-ray treatment.

change in ER structure (Fig. S2 of the supporting information).

3.7. Cell cycle distribution and induction of cell death

Fig. 9 shows the effect of X-ray irradiation without and with ICp_6-Cu treatment on the cell cycle distribution in NT8e and 4451 cells. As compared with the control, ICp_6-Cu treatment alone showed no effect on the cell cycle. X-rays alone and X-rays in combination with ICp_6-Cu treatment led to no change in the fraction of cells in S and G2/M which suggested that these treatments have no effect on cell cycle distribution, *i.e.* no cell cycle arrest. In addition, results also revealed that, compared with X-rays alone, the combined treatment led to a significant increase in apoptosis as indicated by the ∼15% increase in sub-G1 population ($p < 0.05$) [Fig. 9(*b*)].

4. Discussion

ICp_6-Cu is a novel chlorophyll-based PS recently reported by us for potential application in the PDT of cancer (Sarbadhikary *et al.*, 2016). The motivation to synthesize ICp_6-Cu was to exploit the tumor-localizing property of chlorin for multi-modal cancer therapy. One such modality is X-ray photon activation therapy, which in comparison with light-based PDT offers the advantage that the tumor in a deep tissue region can also be treated. Use of metal-based porphyrin can provide an important advantage that the damage to surrounding normal tissue can be minimized due to its selective accumulation in tumor and subsequent localized dose enhancement effect of X-ray photoactivation. Thus, the combined treatment approach may possibly be employed for the treatment of oral cavity cancer where sparing normal tissue architecture and function is important. With this motivation we explored the efficacy of ICp_6-Cu for X-ray photoactivation-induced cytotoxicity in oral cancer cells. Results of our study show that ICp_6-Cu combined with synchrotron X-rays induced significant radiosensitization in the two oral cancer cell lines. At present, the X-ray photoactivation of ICp_6-Cu is performed using an X-ray energy above the *K*-edge absorption of copper (>8.9 keV). Based on the linear absorption coefficient of the soft tissue (Böke, 2014), the estimated half value layer for 9 keV is ∼1 mm (the depth in tissue where the fluence reduces by 50%) which is suitable for only superficial small tumors. The sensitivity enhancement ratio at 20 µ*M* ICp_6-Cu was >1.0 and increased further at higher concentration [Fig. 5(*b*)] due to an increase in cellular uptake (Fig. 2). Interestingly, the radiosensitization effect of ICp_6-Cu was more pronounced in 4451 cells compared with NT8e cells. An important difference

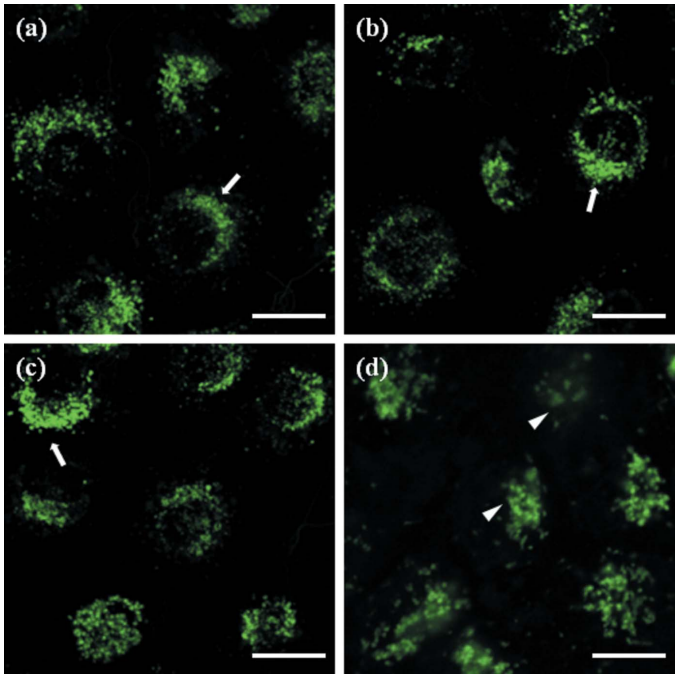

Figure 8
Confocal fluorescence micrographs of NT8e cells showing the effect of ICp_6-Cu-induced radiosensitization on the integrity of lysosomes. Cells were stained with lysosome-specific lysostracker probe. (*a*) Control, (*b*) ICp_6-Cu (30 μ*M*) treatment alone, (*c*) X-ray (7 Gy) treatment alone and (*d*) ICp_6-Cu (30 μ*M*) plus X-ray (7 Gy) treatment. Experiments were repeated three times with similar results and representative images are shown. Arrows indicate intact lysosome; arrow heads indicate weak disintegrated lysosomes. Magnification 40×; scale bar 20 μm.

between the two cell lines is the status of the p53 gene, *i.e.* cell line 4451 has the mutated p53 gene (Zölzer *et al.*, 1995) whereas NT8e has wild-type p53 (Mulherkar *et al.*, 1997). However, the difference in their sensitivity to radiosensitization cannot be attributed to the difference in the status of p53, because the sensitivity of the two cell lines to X-rays alone was almost similar (Fig. 4). The relationship between p53 status and radiosensitivity is not well understood and there are several conflicting reports on radiosensitivity *versus* p53 gene mutation (Anderson *et al.*, 2014; Takahashi *et al.*, 2004; Zhang *et al.*, 2015). As shown in Figs. 2 and 6, the intracellular level of ICp_6-Cu and the relative level of ROS are significantly higher in 4451 cells than for NT8e cells. These results correlated with the higher sensitivity of 4451 cells to ICp_6-Cu-induced radiosensitization and further substantiate the role of photoactivation-induced ROS generation in the radiosensitization effect of ICp_6-Cu. The results are also in agreement with the fact that ROS generated *via* radiolysis of water plays a major role in X-ray-induced cytotoxicity, and the presence of X-ray absorbing metal can further enhance this process (Kobayashi *et al.*, 2010). Here it is important to note that the irradiation of high-*Z* elements is expected to yield better radiosensitization efficacy because they can generate more secondary electrons than by irradiating lower-*Z* elements (Kobayashi *et al.*, 2010). In the present study, the X-ray energy used for photoactivation of ICp_6-Cu was close to the copper *K*-edge absorption. Since ICp_6-Cu also contains iodine, irradiation with the X-ray energy tuned to the iodine

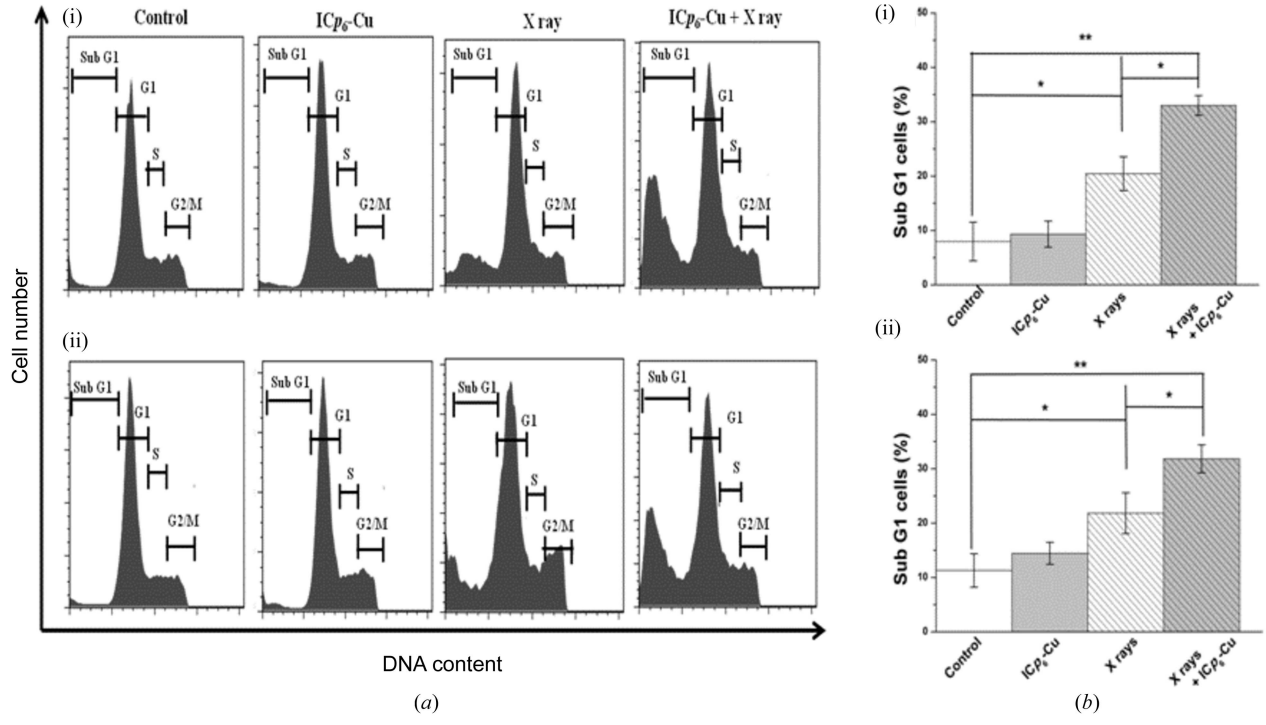

Figure 9
Effect of ICp_6-Cu and X-ray irradiation on cell cycle distribution in NT8e and 4451 at 24 h post-irradiation. (*a*) Cell cycle histograms of NT8e (i) and 4451 (ii) cells. (*b*) Percentage of NT8e (i) and 4451 (ii) cells in sub-G1-phase, for control, ICp_6-Cu treatment alone, X-ray irradiation alone and ICp_6-Cu plus X-ray treatment. The cells were treated with 30 μ*M* ICp_6-Cu for 3 h and then irradiated with X-rays at a fixed dose of 7 Gy. Data represent mean ± standard deviation obtained from three independent experiments. *($p < 0.05$), **($p < 0.01$) indicate statistical significance.

K_α edge (~33 keV) may produce more efficient radiosensitization against cancer cells.

An important mechanism of the radiosensitization effect of currently applied PAT drugs such as cisplatin and 5-iodo-2′-deoxyuridine is the enhancement in DNA damage and/or inhibition of DNA repair which is primarily attributed to the localization of these drugs in the cell nucleus (Turchi *et al.*, 2000; Biston *et al.*, 2009; Bayart *et al.*, 2017). As shown in Fig. 7(*b*), ICp_6-Cu pre-treatment did not lead to any increase in the level of X-ray-induced DSBs which is consistent with the absence of its localization in the cell nucleus (Fig. 3). Interestingly, analysis of γ-H2AX foci at 2 h and 24 h post-irradiation (Fig. 7*c*) revealed that the repair of DSBs is significantly inhibited in ICp_6-Cu treated cells. Previous studies have shown that platinated drugs inhibit or delay X-ray-induced DSBs due to the formation of cisplatin–DNA adducts (Turchi *et al.*, 2000). For, ICp_6-Cu the reason for the inhibition of DNA repair and accumulation of unrepaired DNA is not clear. The observations that ICp_6-Cu localized in lysosomes and combined treatment led to disintegration of lysosomes suggested that, unlike platinum drugs, the radiosensitization effect of ICp_6-Cu involved dose deposition in cytoplasm and damage to vital cell organelles. The formation of free radicals and ROS due to the photoactivation of ICp_6-Cu in lysosomes may lead to inactivation of lytic enzymes and destabilization of these organelles (Persson *et al.*, 2005; Dayal *et al.*, 2014). Lysosomes play an important role in the clearance of damaged DNA through the action of *Dnase2a*, a lysosomal endonuclease that degrades DNA to oligonucleotides and nucleotides. Recent studies have shown that the deficiency of *Dnase2a* results in elevated levels of DSBs subsequent to treatment with DNA-damaging agents (Lan *et al.*, 2014). Moreover, the persistence of unrepaired DSBs has been identified as a potentially lethal event that triggers apoptotic cell death (Roos & Kaina, 2013). Consisitent with this, ICp_6-Cu plus X-ray treatment led to significant increase in sub-G1 population that mainly corresponds to apoptotic cells (Darzynkiewicz *et al.*, 2010).

5. Conclusions

Results demonstrated that ICp_6-Cu through X-ray photoactivation induced potent radiosensitization effect in oral cancer cells. The underlying mechanism of radiosensitization involved photoactivation-induced enhancement in ROS production, damage to lysosomes and subsequent impairment of the ability of cells to repair X-ray-induced DSBs. Since an X-ray energy of 9.0 keV penetrates only a few millimeters in soft tissue, it needs further investigations using X-ray energies tuned to the iodine K_α edge (~33 keV) to establish the efficacy of ICp_6-Cu for the treatment of deep-seated tumors.

Acknowledgements

We would like to thank Dr B. S. Dwarakanath, INMAS, Delhi, and Dr U. M. Warawdekar, ACTREC, Mumbai, for providing the oral cancer cell lines. We are also thankful to Dr V. P. Dhamgaye and Shri. B. S. Thakur for their assistance in carrying out X-ray irradiation experiments at beamline BL7 of the Indus-II synchrotron source at our center. We would like to acknowledge Dr Santosh K. Sandur and Dr Deepak Sharma (BARC) for providing technical support and expert guidance in flow cytometry experiments. PS acknowledges Homi Bhabha National Institute, Mumbai, for a senior research fellowship. Disclosure statement: Alok Dube, Paromita Sarbadhikary and Pradeep Kumar Gupta are named patent inventors for Indian Patent Application No. 4912/MUM/2015 titled ‘A metal complex of chlorophyll derivative for magnetic resonance imaging and photodynamic therapy’, filed on 29 December 2015.

Funding information

The following funding is acknowledged: Department of Atomic Energy, Government of India, Homi Bhabha National Institute, Raja Rammana Centre of Advanced Technology (scholarship No. Senior Research Fellowship to Paromita Sarbadhikary).

References

Abrahamse, H. & Hamblin, M. R. (2016). *Biochem. J.* **473**, 347–364.
Adam, J. F., Biston, M., Rousseau, J., Boudou, C., Charvet, A., Balosso, J., Estève, F. & Elleaume, H. (2008). *Phys. Med.* **24**, 92–97.
Adam, J. F., Joubert, A., Biston, M. C., Charvet, A. M., Peoc'h, M., Le Bas, J. F., Balosso, J., Estève, F. & Elleaume, H. (2006). *Int. J. Radiat. Oncol. Biol. Phys.* **64**, 603–611.
Anderson, D. L., Mirzayans, R., Andrais, B., Siegbahn, E. A., Fallone, B. G. & Warkentin, B. (2014). *J. Synchrotron Rad.* **21**, 801–810.
Astolfi, L., Ghiselli, S., Guaran, V., Chicca, M., Simoni, E., Olivetto, E., Lelli, G. & Martini, A. (2013). *Oncol. Rep.* **29**, 1285–1292.
Bayart, E., Pouzoulet, F., Calmels, L., Dadoun, J., Allot, F., Plagnard, J., Ravanat, J. L., Bridier, A., Denozière, M., Bourhis, J. & Deutsch, E. (2017). *PLoS One*, **12**, e0168395.
Biston, M. C., Joubert, A., Adam, J. F., Elleaume, H., Bohic, S., Charvet, A. M., Estève, F., Foray, N. & Balosso, J. (2004). *Cancer Res.* **64**, 2317–2323.
Biston, M. C., Joubert, A., Charvet, A. M., Balosso, J. & Foray, N. (2009). *Radiat. Res.* **172**, 348–358.
Böke, A. (2014). *Radiat. Phys. Chem.* **102**, 49–59.
Ceresa, C., Nicolini, G., Semperboni, S., Requardt, H., Le Duc, G., Santini, C., Pellei, M., Bentivegna, A., Dalprà, L., Cavaletti, G. & Bravin, A. (2014). *Anticancer Res.* **34**, 5351–5355.
Chapman, J., Stobbe, C., Arnfield, M., Santus, R., Lee, J. & McPhee, M. (1991). *Radiat. Res.* **126**, 73–79.
Chen, H., Wang, G. D., Chuang, Y. J., Zhen, Z., Chen, X., Biddinger, P., Hao, Z., Liu, F., Shen, B., Pan, Z. & Xie, J. (2015). *Nano Lett.* **15**, 2249–2256.
Choi, G. H., Seo, S. J., Kim, K. H., Kim, H. T., Park, S. H., Lim, J. H. & Kim, J. K. (2012). *Radiat. Oncol.* **7**, 184.
Darzynkiewicz, Z., Halicka, H. D. & Zhao, H. (2010). *Adv. Exp. Med. Biol.* **676**, 137–147.
Dayal, R., Singh, A., Pandey, A. & Mishra, K. P. (2014). *J. Cancer Res. Ther.* **10**, 811–818.
Deman, P., Edouard, M., Besse, S., Vautrin, M., Elleaume, H., Adam, J. F. & Estève, F. (2010). *Rev. Med. Interne.* **31**, 586–589.
Engels, E., Lerch, M., Tehei, M., Konstantinov, K., Guatelli, S., Rosenfeld, A. & Corde, S. (2017). *J. Phys. Conf. Ser.* **777**, 012011.
Gil, S., Fernández, M., Prezado, Y., Biete, A., Bravin, A. & Sabés, M. (2011). *Clin. Transl. Oncol.* **13**, 715–720.
Gohary, M. I. El., Shabban, Y. S., Amin, E. A., Abdel Gawad, M. H. & Desouky, O. S. (2015). *Nat. Sci.* **13**, 139–143.

Hainfeld, J. F., Dilmanian, F. A., Slatkin, D. N. & Smilowitz, H. M. (2008). *J. Pharm. Pharmacol.* **60**, 977–985.
Ishibashi, N., Fujiwara, K., Pandey, R. K., Kataba, M., Oguni, A., Igarashi, J., Soma, M., Shizukuishi, T., Maebayashi, T. & Abe, K. (2013). *Nihon Univ. J. Med.* **72**, 212–219.
Kaščáková, S., Giuliani, A., Lacerda, S., Pallier, A., Mercère, P., Tóth, E. & Réfrégiers, M. (2015). *Nano Res.* **8**, 2373–2379.
Kobayashi, K., Usami, N., Porcel, E., Lacombe, S. & Le Sech, C. (2010). *Mutat. Res.* **704**, 123–131.
Lan, Y. Y., Londoño, D., Bouley, R., Rooney, M. S. & Hacohen, N. (2014). *Cell. Rep.* **9**, 180–192.
Liu, Y., Chen, W., Wang, S. & Joly, A. G. (2008). *Appl. Phys. Lett.* **92**, 043901.
Mah, L., El-Osta, A. & Karagiannis, T. (2010). *Leukemia*, **24**, 679–686.
Moan, J. & Sommer, S. (1985). *Cancer Res.* **45**, 1608–1610.
Morgan, N. Y., Kramer-Marek, G., Smith, P. D., Camphausen, K. & Capala, J. (2009). *Radiat. Res.* **171**, 236–244.
Mosmann, T. (1983). *J. Immunol. Methods*, **65**, 55–63.
Mulherkar, R., Goud, A. P., Wagle, A. S., Naresh, K., Mahimkar, M. B., Thomas, S. M., Pradhan, S. & Deo, M. (1997). *Cancer Lett.* **118**, 115–121.
Persson, H. L., Kurz, T., Eaton, J. W. & Brunk, U. T. (2005). *Biochem. J.* **389**, 877–884.
Price, P. & McMillan, T. J. (1990). *Cancer Res.* **50**, 1392–1396.
Rappole, C. A., Mitra, K. & Wen, H. (2012). *Opt Nanoscopy*, **1**, 5.
Ricard, C., Fernandez, M., Requardt, H., Wion, D., Vial, J.-C., Segebarth, C. & van der Sanden, B. (2013). *J. Synchrotron Rad.* **20**, 777–784.
Roos, W. P. & Kaina, B. (2013). *Cancer Lett.* **332**, 237–248.
Rousseau, J., Adam, J.-F., Deman, P., Wu, T.-D., Guerquin-Kern, J.-L., Gouget, B., Barth, R. F., Estève, F. & Elleaume, H. (2009). *J. Synchrotron Rad.* **16**, 573–581.
Sapan, C. V., Lundblad, R. L. & Price, N. C. (1999). *Biotechnol. Appl. Biochem.* **29**, 99–108.
Sarbadhikary, P., Dube, A. & Gupta, P. K. (2016). *RSC Adv.* **6**, 75782–75792.
Su, X. Y., Liu, P. D., Wu, H. & Gu, N. (2014). *Cancer Biol. Med.* **11**, 86–91.
Takahashi, A., Matsumoto, H., Yuki, K., Yasumoto, J. I., Kajiwara, A., Aoki, M., Furusawa, Y., Ohnishi, K. & Ohnishi, T. (2004). *Int. J. Radiat. Oncol. Biol. Phys.* **60**, 591–597.
Taupin, F., Flaender, M., Delorme, R., Brochard, T., Mayol, J. F., Arnaud, J., Perriat, P., Sancey, L., Lux, F., Barth, R. F., Carrière, M., Ravanat, J. L. & Elleaume, H. (2015). *Phys. Med. Biol.* **60**, 4449–4464.
Tsuchida, T., Kato, H., Okunaka, T., Harada, M., Ichinose, S. & Hirata, T. (2003). *Lung Cancer*, **41**, S133.
Turchi, J. J., Henkels, K. M. & Zhou, Y. (2000). *Nucleic Acids Res.* **28**, 4634–4641.
Wang, G. D., Nguyen, H. T., Chen, H., Cox, P. B., Wang, L., Nagata, K., Hao, Z., Wang, A., Li, Z. & Xie, J. (2016). *Theranostics*, **6**, 2295–2305.
Zhang, J., Shen, L. & Sun, L. Q. (2015). *Cancer Lett.* **363**, 108–118.
Zölzer, F., Hillebrandt, S. & Streffer, C. (1995). *Radiother. Oncol.* **37**, 20–28.